Performance Analysis of Downlink Non-Orthogonal Multiple Access under Imperfect CSI in Dense Network: A Stochastic Geometry Approach

Thanh-Luan NGUYEN, Dinh-Thuan DO

Department of Electronics and Telecommunications, Faculty of Electronics Technology,
Industrial University of Ho Chi Minh City, 12 Nguyen Van Bao, 700000 Ho Chi Minh City, Vietnam

nguyenthanhluan@iuh.edu.vn, dodinhthuan@iuh.edu.vn

DOI: 10.15598/aeee.v18i4.3793

Abstract. *A single-tier downlink Non-Orthogonal Multiple Access (NOMA) network is considered in this paper where analytical framework is given for performance evaluation. Particularly, the outage probability at the downlink users is studied under the impact of imperfect Channel State Information (CSI). The inter-cell interference and the intra-cell interference are also taken into consideration to capture practical behaviors of the proposed system. Further, we also adopt the Poisson Point Process (PPP) to model the location of the base stations and the downlink users in this work. For the imperfect CSI scenario, the results point out that the more times the user spends on performing interference cancellation, the more severe the user is affected by channel estimation error and vice versa. The results for the outage probability expressed in the analytical-forms are then confirmed by the Monte Carlo simulations.*

Keywords

Imperfect CSI, NOMA, outage probability, stochastic geometry.

1. Introduction

In recent years, applying Non-Orthogonal Multiple Access (NOMA) in 5G networks has been attracting much attention among researchers [1], [2], [3], and [4]. In specific, NOMA allows multiple users (UEs) share the same radio resources, e.g., frequency/time, by utilizing Superposition Coding (SC) at the transmitters with different allocated powers so that the receivers can extract the desired messages from the superimposed mixture via Successive Interference Cancellation (SIC) [5].

Many studies about NOMA have been reported in the literature. The authors in [6] studied the Power Allocation (PA) strategies that ensure fairness among downlink users. In [7], the authors investigated the performance of downlink NOMA and downlink OMA in multicell network which include a collection of small-cell base station BSs and pointed out that NOMA can achieve higher performance gain comparing to Orthogonal Frequency Division Multiple Access (OFDMA). The authors then extend their work in [8] where both uplink and downlink NOMA in dense small cell networks with two user-pairing strategies, namely random pairing and selective pairing, comparisons of the proposed strategies are also given. Authors of [9] consider imperfect CSI in NOMA assisted single-cell network in terms of outage probability and average rate which shows that NOMA can still achieve higher performance than the conventional Orthogonal Multiple Access technologies (OMA).

In single-tier networks, inter-cell interference contributes as a performance-limiting factor and thus should be carefully studied. To addressed this problem, many stochastic geometry models have been proposed. In [10], authors model the location of the Base Station (BS) in a multicell network using homogeneous Poisson Point Process (PPP) and shown that the performance of homogeneous PPP models is bounded by that of the empirical models. The application of the PPP model to characterize the coverage performance of the wireless network in the UK is studied in [11] where it shows an insignificant difference with the realistic model and proved to be not only

more accurate but also more tractable than the grid-based model [10]. In the application of PPP in NOMA, the authors in [12] adopted multiple Poisson Cluster Processes, which are originated by the baseline homogeneous PPP, to model the uplink NOMA. Further, application in characterizing the impact of multiple types of randomly deployed interference in NOMA is studied in [13]. The works in [8] and [9] also adopt the homogeneous PPP model to study the impact of inter-cell interference in dense small cell network.

In the above works, perfect CSI is assumed in [1], [2], [3], [4], [6], [7], and [8]. Considering imperfect CSI, the work in [9] addressed the dynamic movement of multiple download users inside a circular area. In addition, the recent work in [14] proposed a downlink multi-user NOMA system where the location of users is fixed. It is shown that imperfect CSI affects the performance at each downlink user as stated in [9] and [14].

However, the aforementioned works are limited to a single-cell scenario. For the sake of practical deployment of NOMA in multicell networks, the impact of estimation error should be carefully investigated since estimating the CSI perfectly produces significant overhead, which is extremely severe with a vast amount of small devices. To fill up the gaps in the above works, our motivation is to focus on the impact of imperfect CSI in the downlink NOMA multicell network using stochastic geometry tools and the model in [15], [16], [17], [18], and [19].

Our contributions can be reported as providing system performance by stochastic geometry to indicate the performance of a dense network. We find the closed-form of expression.

The rest of the paper is organized as follows. Section 2. introduces the system model. Section 3. studies the outage performance of the system. In Sec. 4. , we provide simulation to validate the results in Sec. 3. . Finally, Sec. 5. is the conclusion.

2. System Model

This paper studies a NOMA-assisted downlink single tier network comprising a collection of BSs and downlink NOMA users (UEs). The locations of BSs are captured by a Homogeneous PPP (HPPP) with intensity λ_b, denoted by Φ_b, such that:

$$\Phi_b \triangleq \{b_0, b_1, b_2, \ldots, \forall b_i \in \mathbb{R}^2, i \geq 0\}. \quad (1)$$

Now, we assume that the locations of UEs are modeled by independent stationary point processes and each NOMA user is associated with the closest BS, thus UEs are located inside the Voronoi cell of the BSs, forming the Voronoi tessellation as in Fig. 1. Note that the disadvantages and advantages of the underlying HPPP model are already well presented in [10].

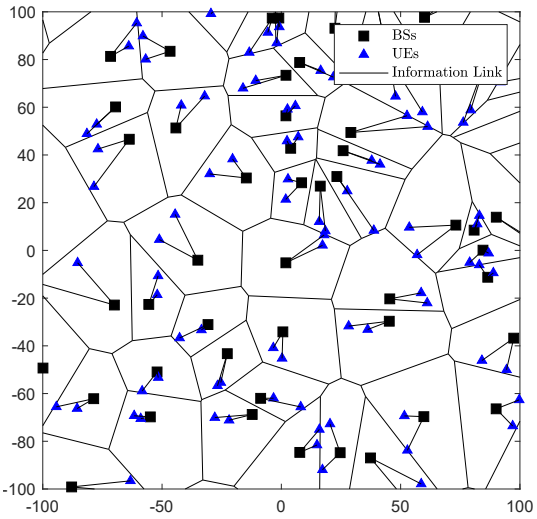

Fig. 1: A realization of the single-tier downlink NOMA with dense deployment of BSs.

Let R_i be the distance between an UE_i and its associated BS and all R_i are independently and identically distributed random variables (r.v.'s) following Rayleigh distribution with mean $\frac{1}{\sqrt{4\lambda_b}}$ [10]. In other words, the Probability Density Function (PDF) of the nearest neighbor distance R_i is given as:

$$f_{R_i}(r) = 2\pi\lambda_b r e^{-\lambda_b \pi r^2}, \; r > 0. \quad (2)$$

Denoting $r_i = h_i R_i^{-\frac{\eta}{2}}$ as the channel between each UE_i and its associated BS, in which h_i follows circular complex Gaussian distribution with zero mean and unit variance, and η denotes the path loss exponent.

In practice, obtaining perfect CSI causes significant overhead at the receivers, not to mention high complexity in the receiver architecture. Hence, the practical imperfect CSI model is adopted in this paper where we assume error-free and instantaneous feedback link [15] and [16]. Assuming Minimum Mean Square Error (MMSE) is adopted for estimating information channels, thus [17], [18], and [19].

$$r_i = \tilde{r}_i + \varepsilon_i, \quad (3)$$

in which $\varepsilon_i \sim CN(0, \sigma_\varepsilon^2)$ is the zero mean complex Gaussian random variable with variance σ_ε^2 reflecting the accuracy of the channel estimation module. The estimated channel $\tilde{r}_i$ is independent with the input channel r_i, where $\mathbb{E}\{|\tilde{r}_i|^2\} = R_i^{-\eta} - \sigma_\varepsilon^2$, $0 \leq \sigma_\varepsilon^2 \leq R_i^{-\eta}$. Denoting $\delta_\varepsilon \triangleq \sigma_\varepsilon^2 R_i^\eta$ as the normalized estimation error, thus $\mathbb{E}\{|\tilde{r}_i|^2\} = R_i^{-\eta}(1 - \delta_\varepsilon)$ with $0 \leq \delta_\varepsilon \leq 1$.

Assuming unit frequency reuse among all cells, thus the inter-cell interference observed in the typical cell

is originated from all other BSs b_k, $\forall k \neq 0$. Hence, the aggregated inter-cell interference received at UE$_i$ located inside the Voronoi cell of the tagged BS $\mathbf{b}_0$ can be modeled as:

$$I_i^{agg} \triangleq \sum_{\forall k \in \frac{\Phi}{b_0}} f_{k,i} R_{k,i}^{-\eta} P_b, \tag{4}$$

in which $f_{k,i} \sim CN(0,1)$ and $R_{k,i}$ denotes the channel coefficient and the distance of the interfering channel from the BS k to UE$_i$, respectively, whereas P_b is the transmit power of all BSs. In this paper, we assume that the UE$_i$ are ordered as:

$$\frac{|\tilde{r}_1|^2}{I_1^{agg}+\sigma^2} \leq \frac{|\tilde{r}_2|^2}{I_2^{agg}+\sigma^2} \leq \cdots \leq \frac{|\tilde{r}_N|^2}{I_N^{agg}+\sigma^2}, \tag{5}$$

where σ^2 denotes the Gaussian noise variance at UE$_i$. Let P_i be the power allocation for the UE$_i$ with $\sum_{i=1}^{N} P_i = 1$. Accordingly, NOMA schemes orders the P_i as $P_1 \geq P_2 \geq \cdots \geq P_N$ to elevate downlink user fairness [6].

2.1. Information Transmission

Considering the typical cell of the BS located at $\mathbf{b}_0 \in \Phi_b$, the analysis inside this cell reflects the spatial average of the entire system according to Slivnyak's theorem for stationary point processes [20]. Let s_i be the unit energy signal intended to UE$_i$, $1 \leq i \leq N$, respectively. According to NOMA principle [1], [2], [3], and [4], the transmitted signal at BS is coded to form the superimposed mixture of UE$_i$'s signals as $x_b = \sum_{i=1}^{N} \sqrt{P_i} s_i$, thus the received signal at UE$_i$ is given by:

$$\begin{aligned} y_i &= \sqrt{P_b} x_b r_i + I_i^{agg} + n_i = \\ &= \underbrace{\sqrt{P_i P_b} x_i \tilde{r}_i}_{\text{information signal}} + \\ &+ \underbrace{\sqrt{P_b} \sum_{k=1, k\neq i}^{N} \sqrt{P_k} s_k \tilde{r}_i + I_i^{agg} + \sqrt{P_b} x_i \varepsilon_i + n_i}_{\text{interference-plus-noise}}, \end{aligned} \tag{6}$$

in which $n_i \sim CN(0,\sigma^2)$ denotes the Gaussian noise with $\mathbb{E}\{n_i\} = 0$ and $\mathbb{E}\{|n_i|^2\} = \sigma^2$.

The decoding process at each UE$_i$ via Successive Interference Cancellation (SIC) is explained as follows. One-by-one, each UE$_i$ decodes the messages of UE$_j$ where $j = 1, 2, \ldots, i$ while being affected by the intra-cell interference from others UE$_t$, $t \in [j+1, N]$. Further, whenever s_j is successfully retrieved, the UE$_i$ subtracts it from y_i. The processes, i.e. the decoding and the canceling of the signal s_j, are looped till s_i is retrieved. Subsequently, the received instantaneous rate at the i-th paired user is given by:

$$R_{j\rightarrow i} = \log_2 \left(1 + \frac{P_b P_j |\tilde{r}_i|^2}{P_b \hat{P}_{j+1} |\tilde{r}_i|^2 + I_i^{agg} + P_b \sigma_\varepsilon^2 + \sigma^2} \right), \tag{7}$$

where $\hat{P}_j = \sum_{k=j}^{N} P_k$ with $2 \leq j \leq N$ and $\hat{P}_{N+1} = 0$.

By denoting $\psi_i \triangleq (|\tilde{r}_i|^2)/(I_i^{agg} + P_b\sigma_\varepsilon^2 + \sigma^2)$ as the ordered Normalized Estimated Channel Power Gain (NECPG) at the UE$_i$, the above equation becomes:

$$R_{j\rightarrow i} = \log_2 \left(1 + \frac{P_j P_b \psi_i}{\hat{P}_{j+1} P_b \psi_i + 1} \right). \tag{8}$$

Further, from Eq. (5) it is predicted that $\psi_1 \leq \psi_2 \leq \cdots \leq \psi_N$.

3. Performance Analysis

3.1. Unordered/Ordered NECPG Distribution

In prior to evaluate the outage at the UE$_i$, the calculations for the Cumulative Distribution Function (CDF) of the unordered NECPG, namely $\bar{\psi}_i$, and the ordered NECPG are required. First, the CDF of the unordered $\bar{\psi}_i$ is given as:

$$\begin{aligned} F_{\bar{\psi}_i}(\psi) &= 1 - \Pr\left\{ \frac{|\tilde{r}_i|^2}{I_i^{agg} + P_b\sigma_\varepsilon^2 + \sigma^2} > \psi \right\} = \\ &= 1 - \mathbb{E}_{R_i, I_i^{agg}} \left\{ \exp\left(-\frac{I_i^{agg} + P_b\sigma_\varepsilon^2 + \sigma^2}{R_i^{-\eta}(1-\delta_\varepsilon)} \psi \right) \right\}. \end{aligned} \tag{9}$$

Using the definition of the expectation operator, $\mathbb{E}_X = \int_0^\infty f_X(x)dx$, thus Eq. (9) can be derived by Eq. (12) at the top of the next page, where $\mathfrak{L}_{I_i^{agg}}(s) = \mathbb{E}\{e^{-sI_i^{agg}}\}$ specifies the Laplace transform of I_i^{agg} at point s and is given by Eq. (5) in [7] as:

$$\mathfrak{L}_{I_i^{agg}}(s) = \exp\left(-\pi\lambda_b (sP_b)^{\frac{2}{\eta}} \int_{(sP_b/r^\eta)^{-\frac{2}{\eta}}}^{\infty} \frac{1}{1+x^{\frac{\eta}{2}}} dx \right). \tag{10}$$

Plugging the above result into Eq. (12) and then applying the change of variable $\zeta = r^2$, the CDF of the unordered NECPG is rewritten as:

$$\begin{aligned} F_{\bar{\psi}_i}(\psi) = 1 - \pi\lambda_b \int_0^\infty \exp\Bigg\{ &-\frac{\delta_\varepsilon}{1-\delta_\varepsilon}\psi P_b - \frac{\psi\sigma^2}{1-\delta_\varepsilon}\zeta^{\frac{\eta}{2}} \\ &-\pi\lambda_b \left[1 + \left(\frac{\psi P_b}{1-\delta_\varepsilon} \right)^{\frac{2}{\eta}} \int_{\left(\frac{\psi P_b}{1-\delta_\varepsilon}\right)^{-\frac{2}{\eta}}}^{\infty} \frac{1}{1+x^{\frac{\eta}{2}}} dx \right] \zeta \Bigg\} d\zeta. \end{aligned} \tag{11}$$

$$F_{\bar{\psi}_i}(\psi) = 1 - \int_{r>0}\int_{z>0} \exp\left(-\frac{z + P_b\delta_\varepsilon r^{-\eta} + \sigma^2}{r^{-\eta}(1-\delta_\varepsilon)}\psi\right) f_{I_i^{agg}}(z)dz f_{R_i}(r)dr = \\ = 1 - \int_{r>0} \exp\left(-\frac{P_b\delta_\varepsilon r^{-\eta} + \sigma^2}{r^{-\eta}(1-\delta_\varepsilon)}\psi\right) \mathfrak{L}_{I_i^{agg}}\left(\frac{\psi}{r^{-\eta}(1-\delta_\varepsilon)}\right) f_{R_i}(r)dr, \tag{12}$$

In general, the above Eq. (11) cannot be further evaluated in closed-form with all possible values of η. However, with $\eta = 4$, the second integral part can be simplified as:

$$\int_{\left(\frac{\psi P_b}{1-\delta_\varepsilon}\right)^{-\frac{2}{\eta}}}^{\infty} \frac{1}{1+x^{\frac{\eta}{2}}}dx \overset{\eta=4}{=} \arctan\left(\sqrt{\frac{\psi P_b}{1-\delta_\varepsilon}}\right), \tag{13}$$

and then adopting Eq. (2.3.15.4) in [21], the unordered NECPG can then have the closed-form as:

$$F_{\bar{\psi}_i}(\psi) = 1 - \frac{\pi\sqrt{\pi}\lambda_b}{R(\psi)}\text{erfc}\left\{\frac{Q(\psi)}{R(\psi)}\right\} \cdot \\ \cdot \exp\left\{-\frac{\delta_\varepsilon}{1-\delta_\varepsilon}\psi P_b + \left(\frac{Q(\psi)}{R(\psi)}\right)^2\right\}, \tag{14}$$

in which $\text{erfc}(x) = 1 - \frac{2}{\sqrt{\pi}}\int_0^x e^{-z^2}dz$ denotes the complementary error function, $R(\psi) \triangleq 2\sqrt{\frac{\psi\sigma^2}{1-\delta_\varepsilon}}$ and:

$$Q(\psi) \triangleq \pi\lambda_b\left[1 + \sqrt{\frac{\psi P_b}{1-\delta_\varepsilon}}\arctan\left(\sqrt{\frac{\psi P_b}{1-\delta_\varepsilon}}\right)\right]. \tag{15}$$

Utilizing the above results, the CDF of the ordered NECPG measured at ψ can then be derived by the Eq. (9) in [22] as:

$$F_{\psi_i}(\psi) = 1 - \sum_{v=1}^{i} \wp_{v,i}(1 - F_{\bar{\psi}_i}(\psi))^{N-v+1}, \tag{16}$$

in which:

$$\wp_{v,i} = (-1)^{i-v}\binom{N}{i}\binom{i-1}{i-v}\frac{i}{N-v+1}. \tag{17}$$

3.2. Outage Probability

In downlink NOMA systems, the outage probability at the receiver is defined as the probability it decodes its own information signal. In other words, the probability at UE_i is defined via the event UE_i cannot recover its own message s_i, which occurs whenever $R_{j\to\, i}$ falls below the decoding threshold of s_j, denoted as $\bar{R}_i$ (bits·s^{-1}/suband) where $j = 1, 2, \ldots, i$. Mathematically speaking, this probability is formulated as:

$$P_{\text{UE}_i}^{outg} = \Pr\left\{\bigcup_{k=1}^{i} R_{k\to\, i} < \bar{R}_k\right\}. \tag{18}$$

Using the set intersection notation, one can reduce $P_{\text{UE}_i}^{outg}$ as:

$$P_{\text{UE}_i}^{outg} = 1 - \Pr\left\{\bigcap_{j=1}^{i} R_{j\to\, i} \geq \bar{R}_j\right\}, \\ \overset{(a)}{=} 1 - \Pr\left\{\psi_i \geq \frac{1}{P_b}\max_{\forall j\in[1,i]}\left(\frac{\tau_j}{P_j - \tau_j\hat{P}_{j+1}}\right)\right\}, \\ \overset{(b)}{=} F_{\psi_i}\left(\max_{\forall j\in[1,i]}\left(\frac{\tau_j}{P_j - \tau_j\hat{P}_{j+1}}\right)\frac{1}{P_b}\right), \tag{19}$$

where $\tau_j < \frac{P_j}{\hat{P}_{j+1}}$ for $j \in [1,i]$, $\tau_j \triangleq 2^{\bar{R}_j} - 1$, (a) is obtained by substituting Eq. (8) into Eq. (19) with some algebraic steps whereas (b) is due to the definition of the cdf.

4. Simulation Results and Discussion

The section aims to provide numerical examples for the outage performance of the model. In Fig. 2 and Fig. 3, the number of paired users is set to 2. In this section, the simulation results for $P_{\text{UE}_i}^{outg}$ are obtained from Eq. (19) with $R_{j\to\, i}$ in Eq. (7) and average over $5\cdot10^4$ iterations. Accordingly, the analytical results for $\eta = 4$ are from Eq. (19) in which the cdf of the ordered and the unordered NECPG, $F_{\psi_i}(\psi)$ and $F_{\bar{\psi}_i}(\psi)$, are given by Eq. (8) and Eq. (18), respectively. For $\eta \neq 4$, the cdf $F_{\bar{\psi}_i}(\psi)$ in Eq. (11) is adopted. Other default settings are introduced in Tab. 1.

Tab. 1: Default settings.

Parameter	Value
Carrier frequency	2 GHz
Bandwidth	20 MHz
Noise power density	-84 dBm·Hz^{-1}
Pathloss exponent	4
Density of the base station	10^{-3}·m^{-2}
Transmit power of each BS	0 dBm

Figure 2 and Fig. 3 present the outage probability $P_{\text{UE}_1}^{outg}$ and $P_{\text{UE}_2}^{outg}$ under two values of the normalized estimation error, i.e., $\delta_\varepsilon = -10$ dB and $\delta_\varepsilon = -20$ dB. From the provided figures, it is shown that the analytical and the simulation formulas are matched well with each other, which validates our analysis.

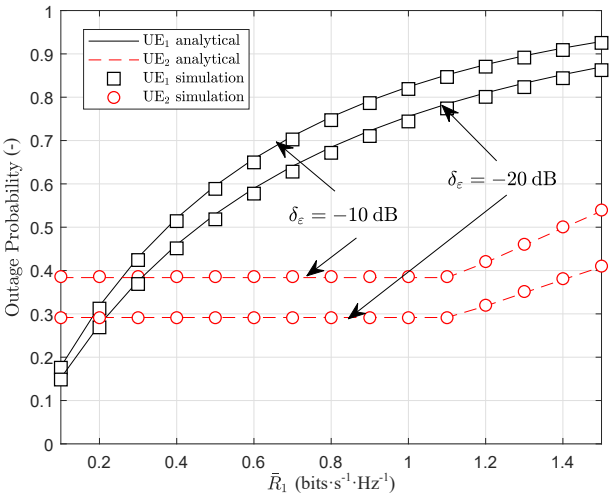

Fig. 2: Outage probability at each UE_i with $N = 2$, $\bar{R}_2 = 0.2$ bits·s^{-1}·Hz^{-1} and $P_1 = 0.9$.

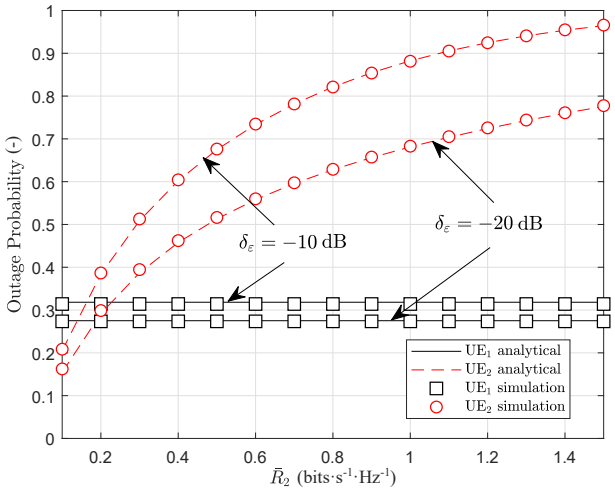

Fig. 3: Outage probability at each UE_i with $N = 2$, $\bar{R}_1 = 0.2$ bits·s^{-1}·Hz^{-1} and $P_1 = 0.9$.

To explain the behaviors of $P_{\text{UE}_2}^{outg}$ in terms of $\bar{R}_1$ in Fig. 2, we then go over Eq. (19) which shows that $P_{\text{UE}_1}^{outg}$ and $P_{\text{UE}_2}^{outg}$ are the functions of $\frac{\tau_1}{P_1 - P_2\tau_1}$ and $\max(\frac{\tau_1}{P_1 - P_2\tau_1}, \frac{\tau_2}{P_2})$, respectively. Further, under the provided settings, we have $\frac{\tau_2}{P_2} \approx 1.49$ and $\frac{\tau_1}{P_1 - P_2\tau_1} \approx 0.08$–$2.55$ with $\bar{R}_1 = 0.1$–1.5 bits·s^{-1}·Hz^{-1}. Accordingly, when $\bar{R}_1 < 1.12$ bits·s^{-1}·Hz^{-1}, $\max(\frac{\tau_1}{P_1 - P_2\tau_1}, \frac{\tau_2}{P_2}) = \frac{\tau_2}{P_2}$ which makes $P_{\text{UE}_2}^{outg}$ independent of $\bar{R}_1$ and thus results in an invariant outage probability at UE_2 in the regime $\bar{R}_1 = 0.1$–1.12 bits·s^{-1}·Hz^{-1}. As $\bar{R}_1$ increases beyond the previous values, i.e., $\bar{R}_1 > 1.12$ bits·s^{-1}·Hz^{-1}, both $P_{\text{UE}_1}^{outg}$ and $P_{\text{UE}_2}^{outg}$ then vary accordingly. In Fig. 3, as $\bar{R}_2$ increases from 0.1 bits·s^{-1}·Hz^{-1} to 1.5 bits·s^{-1}·Hz^{-1}, $\max(\frac{\tau_1}{P_1 - P_2\tau_1}, \frac{\tau_2}{P_2}) = \frac{\tau_2}{P_2} = 0.72$–$18.28$, thus making $P_{\text{UE}_2}^{outg}$ solely depends on $\bar{R}_2$ and independent of $\bar{R}_1$ whereas $P_{\text{UE}_1}^{outg}$ only depends on $\bar{R}_1$ regardless of $\bar{R}_2$ being varied. Hence, as observed, the outage performance at UE_2 deteriorates dramatically, whereas that at UE_1 remains unchanged.

In addition to the impact of target data rates, different values of δ_ε also affect the performance at both UEs. However, the impact of estimation error on UE_2, i.e., the user with higher NECPG, is more severe than on UE_1, as observed from both Fig. 2 and Fig. 3. The reason is that estimation error presents when the UE_2 decodes both s_1 and s_2 whereas it only presents one time at UE_1, i.e., when this user decodes its own message. Hence, it can be predicted with $N \geq 2$, the impact from incorrect channel estimation is dominant at the UE_N and less severe at UE_{N-1} and so on whereas UE_1 will be affected the least.

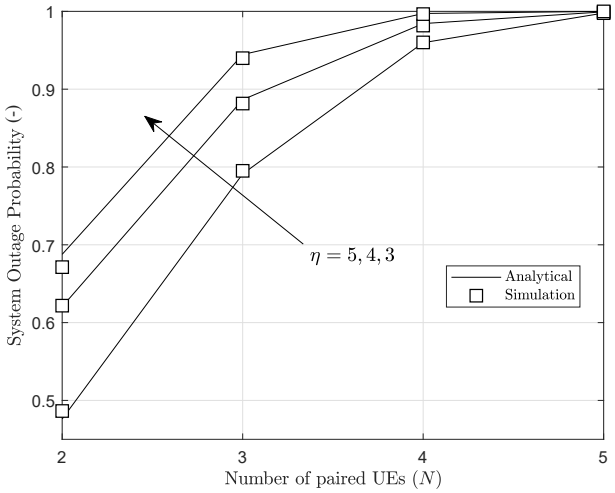

Fig. 4: Outage probability versus the number of paired users (N) where $\bar{R}_i = 0.2$ bits·s^{-1}·Hz^{-1} and $\delta_\varepsilon = -10$ (dB).

In Fig. 4, the system outage probability is defined as $1 - \prod_{i=1}^{N}(1 - P_{\text{UE}_i}^{outg})$ with the PA coefficient at each user is $P_i = \frac{(2^{N-i+1}-1)}{\sum_{i=1}^{N}(2^i - 1)}$. It is observed that higher value of η results in better system performance. The main reason is that although higher path loss degrades the estimated channel power gain at each UE, it also significantly reduces the impact of inter-cell interference on the UEs. Further, as the number of paired UEs, the system performance tends to reach one, whereas $N = 2$ is the optimal value.

5. Conclusion

In this paper, the outage probability of NOMA is evaluated with the aid of the stochastic geometry method. The derived results expressed both in integral-form and closed-form are validated via Monte Carlo simulations, which can be scaled up to the N-UE NOMA case with $N \geq 2$. Our study shows that by considering inter-cell interference, the performance of the system is degraded with a higher path loss exponent due to the high interference level at each UE. Moreover, the user that spends more time for SIC would be more severely affected by channel estimation error.

References

[1] SAITO, Y., Y. KISHIYAMA, A. BENJEBBOUR, T. NAKAMURA, A. LI and K. HIGUCHI. Non-Orthogonal Multiple Access (NOMA) for Cellular Future Radio Access. In: *2013 IEEE 77th vehicular technology conference (VTC Spring)*. Dresden: IEEE, 2013, pp. 1–5. ISBN 978-1-4673-6337-2. DOI: 10.1109/VTCSpring.2013.6692652.

[2] DING, Z., Z. YANG, P. FAN. and H. V. POOR. On the Performance of Non-Orthogonal Multiple Access in 5G Systems with Randomly Deployed Users. *IEEE Signal Processing Letters*. 2014, vol. 21, iss. 12, pp. 1501–1505. ISSN 1558-2361. DOI: 10.1109/LSP.2014.2343971.

[3] HIGUCHI, K. and A. BENJEBBOUR. Non-orthogonal Multiple Access (NOMA) with Successive Interference Cancellation for Future Radio Access. *IEICE Transactions on Communications*. 2015, vol. 98, iss. 3, pp. 403–414. ISSN 1745-1345. DOI: 10.1587/transcom.E98.B.403.

[4] BENJEBBOUR, A., Y. SAITO, Y. KISHIYAMA, A. LI, A. HARADA and T. NAKAMURA. Concept and practical considerations of non-orthogonal multiple access (NOMA) for future radio access. In: *2013 International Symposium on Intelligent Signal Processing and Communication Systems*. Naha: IEEE, 2013, pp. 770–774. ISBN 978-1-4673-6361-7. DOI: 10.1109/ISPACS.2013.6704653.

[5] HASNA, M. O., M.-S. ALOUINI, A. BASTAMI and E. S. EBBINI. Performance analysis of cellular mobile systems with successive co-channel interference cancellation. *IEEE Transactions on Wireless Communications*. 2003, vol. 2, iss. 1, pp. 29–40. ISSN 1558-2248. DOI: 10.1109/TWC.2002.806359.

[6] TIMOTHEOU, S. and I. KRIKIDIS. Fairness for Non-Orthogonal Multiple Access in 5G Systems. *IEEE Signal Processing Letters*. 2015, vol. 22, iss. 10, pp. 1647–1651. ISSN 1558-2361. DOI: 10.1109/LSP.2015.2417119.

[7] ZHANG, Z., H. SUN, R. Q. HU and Y. QIAN. Stochastic Geometry Based Performance Study on 5G Non-Orthogonal Multiple Access Scheme. In: *2016 IEEE Global Communications Conference (GLOBECOM)*. Washington, DC: IEEE, 2016, pp. 1–6. ISBN 978-1-5090-1328-9. DOI: 10.1109/GLOCOM.2016.7842300.

[8] ZHANG, Z., H. SUN and R. Q. HU. Downlink and Uplink Non-Orthogonal Multiple Access in a Dense Wireless Network. *IEEE Journal on Selected Areas in Communications*. 2017, vol. 35, iss. 12, pp. 2771–2784. ISSN 1558-0008. DOI: 10.1109/JSAC.2017.2724646.

[9] YANG, Z., Z. DING, P. FAN and G. K. KARAGIANNIDIS. On the Performance of Non-orthogonal Multiple Access Systems With Partial Channel Information. *IEEE Transactions on Communications*. 2016, vol. 64, iss. 2, pp. 654–667. ISSN 1558-0857. DOI: 10.1109/TCOMM.2015.2511078.

[10] ANDREWS, J. G. ,F. BACCELLI and R. K. GANTI. A Tractable Approach to Coverage and Rate in Cellular Networks. *IEEE Transactions on communications*. 2011, vol. 59, iss. 11, pp. 3122–3134. ISSN 1558-0857. DOI: 10.1109/TCOMM.2011.100411.100541.

[11] LU, W. and M. D. RENZO. Stochastic Geometry Modeling of Cellular Networks: Analysis, Simulation and Experimental Validation. In: *Proceedings of the 18th ACM International Conference on Modeling, Analysis and Simulation of Wireless and Mobile Systems*. Cancun: ACM Press, 2015, pp. 179–188. ISBN 978-1-4503-3762-5. DOI: 10.1145/2811587.2811597.

[12] TABASSUM, H., E. HOSSAIN and J. HOSSAIN. Modeling and Analysis of Uplink Non-Orthogonal Multiple Access in Large-Scale Cellular Networks Using Poisson Cluster Processes. *IEEE Transactions on Communications*. 2017, vol. 65, iss. 8, pp. 3555–3570. ISSN 1558-0857. DOI: 10.1109/TCOMM.2017.2699180.

[13] DO, D.-T., T.-L. NGUYEN and B. M. LEE. Transmit Antenna Selection Schemes for NOMA with Randomly Moving Interferers in Interference-Limited Environment. *Electronics*. 2020, vol. 9, iss. 1, pp. 1–15. ISSN 2079-9292. DOI: 10.3390/electronics9010036.

[14] JIANG, H., Y. WANG, X. YUE and X. LI. Performance analysis of NOMA-based mobile edge computing with imperfect CSI. *EURASIP Journal on Wireless Communications and Networking*. 2020, vol. 1, iss. 1, pp. 1–16. ISSN 1687-1499. DOI: 10.1186/s13638-020-01750-0.

[15] YOO, T. and A. GOLDSMITH. Capacity and power allocation for fading MIMO channels with channel estimation error. *IEEE Transactions on Information Theory*. 2006, vol. 52, iss. 5, pp. 2203–2214. ISSN 1557-9654. DOI: 10.1109/TIT.2006.872984.

[16] HAN, S., S. AHN, E. OH and D. HONG. Effect of Channel-Estimation Error on BER Performance in Cooperative Transmission. *IEEE Transactions on Vehicular Technology*. 2009, vol. 58, iss. 4, pp. 2083–2088. ISSN 1939-9359. DOI: 10.1109/TVT.2008.2007644.

[17] SALAMA, S. I. and S. AISSA. Two-Way Amplify-and-Forward Relaying with Gaussian Imperfect Channel Estimations. *IEEE Communications Letters*. 2012, vol. 16, iss. 7, pp. 956–959. ISSN 1558-2558. DOI: 10.1109/LCOMM.2012.050912.120103.

[18] WANG, C., T. C.-K. LIU and X. DONG. Impact of Channel Estimation Error on the Performance of Amplify-and-Forward Two-Way Relaying. *IEEE Transactions on Vehicular Technology*. 2012, vol. 61, iss. 3, pp. 1197–1207. ISSN 1939-9359. DOI: 10.1109/TVT.2012.2185964.

[19] MA, Y. and J. JIN. Effect of Channel Estimation Errors on M-QAM With MRC and EGC in Nakagami Fading Channels. *IEEE Transactions on Vehicular Technology*. 2007, vol. 56, iss. 3, pp. 1239–1250. ISSN 1939-9359. DOI: 10.1109/TVT.2007.895491.

[20] STOYAN, D., W. S. KENDALL and J. MECKE. *Stochastic Geometry and Its Applications*. 2nd ed. New York: John Wiley & Sons, 1995. ISBN 978-0-471-90519-6.

[21] A. P. PRUDNIKOV, Y. A. BRYCHKOV and O. I. MARICHEV. *Integrals and Series*. 1st ed. Cleveland: CRC Press, 1992. ISBN 978-2-881-24837-5.

[22] NGUYEN, T.-L., C.-B. LE and D.-T. DO. Performance analysis of multi-user NOMA over $\alpha - \kappa - \mu$ shadowed fading. *Electronics Letters*. 2020, vol. 56, iss. 15, pp. 771–773. ISSN 1350-911X. DOI: 10.1049/el.2019.4265.

About Authors

Thanh-Luan NGUYEN received his First class B.Sc. from Ho Chi Minh City University of Technology and Education, Viet Nam, 2016. He currently is a Research Assistant in Industrial University of Ho Chi Minh City (IUH), Faculty of Electronics Technology. His research interests include NOMA, Energy Harvesting, Generalized Channels and other emerging technologies.

Dinh-Thuan DO (Senior Member, IEEE) (Corresponding author) received the B.Sc. degree, M.Eng. degree, and Ph.D. degree from Viet Nam National University (VNU-HCM) in 2003, 2007, and 2013 respectively, all in Communications Engineering. He was a visiting Ph.D. student with Communications Engineering Institute, National Tsing Hua University, Taiwan from 2009 to 2010. Prior to joining Ton Duc Thang University, he was senior engineer at the VinaPhone Mobile Network from 2003 to 2009. Dr. Thuan was recipient of Golden Globe Award from Vietnam Ministry of Science and Technology in 2015 (Top 10 excellent young scientists nationwide). His research interest includes signal processing in wireless communications network, cooperative communications, Non-Orthogonal Multiple Access, full-duplex transmission and energy harvesting. He published over 85 SCI/SCIE journal papers, 4 book chapters and 1 sole author book. Dr. Thuan is currently serving as an Associate Editor in 7 journals, in which main SCIE journals are EURASIP Journal on Wireless Communications and Networking, Computer Communications (Elsevier), Electronics and KSII Transactions on Internet and Information Systems.